

SECURITY INFORMATION

~~SECRET~~

Copy 4
RM L51G10

UNCLASSIFIED
SEP 4 1951

UNCLASSIFIED

NACA

I.N. 5890

UNCLASSIFIED

RESEARCH MEMORANDUM

AN INVESTIGATION OF THE LONGITUDINAL CHARACTERISTICS OF
THE X-3 CONFIGURATION WITH WING AND HORIZONTAL TAIL

~~FOR REFERENCE~~ SURFACES OF ASPECT RATIO 3.0 BY MEANS OF
ROCKET-PROPELLED MODELS

NOT TO BE TAKEN FROM THIS ROOM

RESULTS AT HIGH LIFT COEFFICIENTS

By Robert F. Peck and Jesse L. Mitchell
CLASSIFICATION CHANGED

Langley Aeronautical Laboratory

CONFIDENTIAL Langley Field, Va.

By authority of *NACA Release Form* *August 3, 1953*
Mr. 1545
dated July 27, 1953
This document contains classified information affecting the National Defense of the United States within the meaning of the Espionage Act, USC 50-31 and 32. Its transmission or the revelation of its contents in any manner to an unauthorized person is prohibited by law.
Information so classified may be imparted only to persons in the military and naval services of the United States, appropriate civilian officers and employees of the Federal Government who have a legitimate interest therein, and to United States citizens of known loyalty and discretion who of necessity must be informed thereof.

NATIONAL ADVISORY COMMITTEE FOR AERONAUTICS

WASHINGTON

August 27, 1951

~~SECRET~~

~~CONFIDENTIAL~~

UNCLASSIFIED

~~SECURITY INFORMATION~~

CLASSIFICATION CHANGED

UNCLASSIFIED

By authority of *NACA Release Form* *August 3, 1953*
Mr. 1545
dated July 27, 1953
Date 7/17/58

NACA RM L51G10



3 1176 01436 4393

1 NACA RM L51G10

NATIONAL ADVISORY COMMITTEE FOR AERONAUTICS

RESEARCH MEMORANDUM

AN INVESTIGATION OF THE LONGITUDINAL CHARACTERISTICS OF
THE X-3 CONFIGURATION WITH WING AND HORIZONTAL TAIL
SURFACES OF ASPECT RATIO 3.0 BY MEANS OF
ROCKET-PROPELLED MODELS

RESULTS AT HIGH LIFT COEFFICIENTS

By Robert F. Peck and Jesse L. Mitchell


SUMMARY

A rocket-propelled model of the X-3 configuration equipped with an all-movable tail of aspect ratio 3.0 has been flown to determine the longitudinal characteristics of this configuration at high lift coefficients. An analysis of the response of the model to rapid deflections of the horizontal tail gave information on lift, drag, longitudinal stability, and longitudinal trim change.

The primary result of the tests was that the configuration was indicated to have very unstable tendencies at lift coefficients above the stall and at a Mach number near 0.7. Data obtained at lower lift coefficients in general agreed well with data from a previous model test.

INTRODUCTION

A test program is being conducted by the Pilotless Aircraft Research Division of the NACA to determine longitudinal stability and control characteristics and drag of the X-3 configuration. This research is being done through the use of rocket-propelled free-flight models. This paper contains information obtained from the second X-3 rocket-powered model equipped with an all-movable tail. The primary purpose of this particular test was to investigate the characteristics of the X-3 configuration (with horizontal tail of aspect ratio 3.0) near and above the stall lift coefficient at high-subsonic Mach numbers.



As in the case of the model reported in reference 1, longitudinal aerodynamic characteristics were obtained from measurements made during the free-pitching oscillations following abrupt changes in incidence of an all-movable horizontal tail. Primary differences between the present and previous model (without regard to instrumentation changes) were in center-of-gravity position and values of tail incidence used. The present model attained a maximum Mach number of 1.21. The model was flown at the Langley Pilotless Aircraft Research Station, Wallops Island, Va.

SYMBOLS

C_L	lift coefficient $(C_N \cos \alpha - C_c \sin \alpha)$
C_D	drag coefficient $(C_c \cos \alpha + C_N \sin \alpha)$
C_N	normal-force coefficient $(a_n W / g S q)$
C_c	chord-force coefficient $(-a_t W / g S q)$
C_m	pitching-moment coefficient
a_n/g	normal accelerometer reading
a_t/g	longitudinal accelerometer reading
a_t/g	average reading of transverse accelerometers
W	weight, pounds
S	wing area (including area enclosed within fuselage), square feet
I	moment of inertia in pitch, slug-feet ²
q	dynamic pressure, pounds per square foot
α	angle of attack, degrees
θ	angle of pitch, degrees
$\dot{\alpha}$	rate of change of angle of attack, degrees per second
$\dot{\gamma}$	rate of change of flight-path angle, degrees per second

$\dot{\theta}$	rate of change of angle of pitch, degrees per second
$\ddot{\theta}$	angular acceleration in pitch, degrees per second per second
$\dot{\phi}$	roll velocity, radians per second
$\dot{\psi}$	yaw velocity, radians per second
R	Reynolds number based on wing mean aerodynamic chord
M	Mach number
δ	horizontal tail deflection, degrees
t	time, seconds
$T_{1/2}$	time to damp to one-half amplitude, seconds
C_n	yawing-moment coefficient
β	sideslip angle, degrees
\bar{c}	wing mean aerodynamic chord, feet
K_1	$\frac{I}{qS\bar{c}} \frac{2V}{\bar{c}} \frac{32.2qS}{WV}$
K_2	$\frac{I}{qS\bar{c}} \frac{2V}{\bar{c}} \frac{2 \log_e 1/2}{57.3}$
V	velocity, feet per second

Subscripts:

$\dot{\alpha}$	$\frac{d\alpha}{dt} \frac{\bar{c}}{2V}$, degrees
q	$\frac{d\theta}{dt} \frac{\bar{c}}{2V}$, degrees

The symbols α , q , $\dot{\alpha}$, and β used as subscripts indicate the derivative of the quantity with respect to the subscript, for example

$$C_{L_\alpha} = \frac{\partial C_L}{\partial \alpha}$$

MODEL AND APPARATUS

The X-3 configuration tested had a slender fuselage with dual air inlets located near the top of the fuselage and a 4.5-percent-thick straight wing of aspect ratio 3.0 and taper ratio 0.4. Horizontal and vertical tail surfaces were mounted on a boom behind the fuselage. Details of the model are shown in figures 1, 2, and 3. Use of the bent angle-of-attack-indicator sting provided a means of measuring angle of attack up to 25° with the standard indicator which had a range of $\pm 15^\circ$ relative to the sting. The model was propelled by a Deacon rocket booster. The model and booster on the launcher are shown in figure 4.

The model which is structurally identical to the model described in reference 1 was of all-metal construction. The body was made of magnesium castings and duralumin sheet and wing and tail surfaces were solid duralumin.

As in the case of the model of reference 1, a simple air-induction system was incorporated in the model to give a mass-flow ratio of approximately 0.8 through the inlets. These inlets were connected to constant-diameter ducts designed for choked flow at the exits.

A hydraulic accumulator provided power to pulse the horizontal tail in a square wave pattern between deflections of approximately -1.6° and -4.2° during the coasting part of the flight. An NACA telemetering system provided continuous information on free-stream total pressure, calibrated static pressure (measured at base of angle-of-attack-indicator cone), normal acceleration, longitudinal acceleration, transverse acceleration at two points in the model (on each side of fuselage), angle of attack and horizontal tail position. The Doppler velocimeter, NACA modified SCR 584 tracking radar and radisonde were used to check free-stream conditions at the model during the early part of the flight.

The weight of the model was 139.6 pounds, the center of gravity was 0.4 percent back of the leading edge of the wing mean aerodynamic chord, and the moment of inertia in pitch was 15.9 slug-feet squared.

The primary differences in this model and the model of reference 1 were in center-of-gravity location and tail deflections used. The center of gravity of the model of reference 1 was 15 percent ahead of the leading edge of wing mean aerodynamic chord and the tail was deflected between nominal values of 0° and -2.7° .

The Reynolds number of the test (based on wing mean aerodynamic chord) is shown in figure 5.

TEST AND ANALYSIS PROCEDURE

The test technique employed in obtaining these data was that of oscillating the model in pitch by means of an all-movable horizontal tail while the model decelerated through the Mach number range. The response of the model to the disturbance was measured by means of instruments in the model and was transmitted to the ground by means of a telemeter.

During the early part of the coasting flight, time histories of Mach number, velocity, dynamic pressure, Reynolds number, lift coefficient, drag coefficient, angle of attack, control position, periods of the oscillations due to control disturbance, and time for the oscillation to damp to one-half amplitude were obtained from the telemetered information.

These data were then analyzed by methods discussed in reference 2 to obtain the variation with Mach number of longitudinal stability, control, trim, and drag of the configuration.

The variation of pitching-moment coefficient with angle of attack for the model at a Mach number of approximately 0.7 was obtained by graphically measuring the rate of change of angle of attack $\dot{\alpha}$ from the angle-of-attack time history and by calculating the rate of change of flight-path angle $\dot{\gamma}$ from the time history of lift coefficient (gravity was neglected). These values were added together to obtain the rate of change of the angular position of the model longitudinal axis in space $\dot{\theta}$. The time history of $\dot{\theta}$ was then used to obtain graphically θ which was proportional to the total pitching-moment coefficient. The pitching-moment coefficient due to damping was estimated by using the damping coefficient $C_{mq} + C_{m\dot{\alpha}}$ obtained from the tests of reference 1 and by assuming $C_{mq} = 2C_{m\dot{\alpha}}$. The pitching-moment coefficient due to damping was then subtracted from the total coefficient to obtain the static pitching-moment coefficient C_m due to angle of attack.

At 8.9 seconds after firing, the angle-of-attack indicator range was exceeded (that is, angle of attack exceeded 25°). After this time, because of the effects of very high angles of attack on the pressure measuring devices used on the model it was not possible to obtain accurate values of Mach number and dynamic pressure. Therefore the coefficients C_L , C_D , and so forth were not obtained. During the time interval between 8.9 and 12.0 seconds, however, time histories of the accelerations were obtained along with a measure of the roll and yaw velocities. Roll and yaw velocities could not be obtained separately

but the sum of the roll velocity squared plus the yaw velocity squared, $(\dot{\phi})^2 + (\dot{\psi})^2$, was obtained from the transverse accelerometers. The two transverse accelerometers were mounted on opposite sides of the fuselage. Total acceleration read at each of these points at any time was the sum of accelerations due to pure side forces on the model, centripetal accelerations at the accelerometer due to rolling velocity and centripetal accelerations at the accelerometer due to yawing velocity. Pure lateral accelerations were obtained by averaging the accelerometer readings (subject to errors discussed in the Accuracy and Corrections section of this report) and the total centripetal acceleration effects were obtained by taking the difference in the readings. This difference was proportional to the aforementioned quantity $(\dot{\phi})^2 + (\dot{\psi})^2$.

ACCURACY AND CORRECTIONS

From a consideration of possible zero shifts in the telemetered data of 1 to 2 percent of full-scale instrument range and on the basis of limited independent checks of the Mach number and static pressure the limits of accuracy of some of the important quantities obtained from the flight test are believed to be as follows:

Quantities	Mach number			
	1.15	1.00	0.85	0.7
C_L	± 0.016	± 0.022	± 0.032	± 0.050
$C_{D_{min}}$	± 0.0012	± 0.0017	± 0.0025	± 0.0038
α	$\pm .5$	$\pm .5$	$\pm .5$	$\pm .5$
δ	$\pm .15$	$\pm .15$	$\pm .15$	$\pm .15$
M	$\pm .01$	$\pm .01$	$\pm .02$	$\pm .02$

In addition the absolute angle of attack may be further in error because of undetermined aerodynamic asymmetry effects of the free-floating vane used to measure angle of attack. These asymmetry effects may or may not compensate for the possible error of $\pm 0.5^\circ$ in angle of attack listed previously.

The aforementioned errors affect only the absolute magnitude of the measured quantities and, consequently, have only minor effects on both the trends indicated by the measurements and on slopes and incremental quantities derived from the measurements.

The indicated angle of attack was corrected for position error (during coasting flight previous to 8.9 seconds) by the method described in reference 3. All the accelerometers were mounted in such a position that their position errors would arise only from yawing and rolling motions. Until the angle-of-attack-indicator range was exceeded (at 8.9 seconds after firing) these types of motion were of very small magnitude and caused no measurable position error in the measurements made by these instruments. However between 8.9 and 11.0 seconds measurements of longitudinal, normal and transverse accelerations were subject to measurable position errors. Position errors during this interval of time could not be calculated exactly but were estimated to be the order of 1 to 2g.

DISCUSSION

Time Histories

As pointed out previously the basic data were obtained in the form of time histories. In figure 6 is presented a qualitative time-history plot illustrating the response of the model to the elevator deflections during the portion of coasting flight up to 8.9 seconds after firing.

Oscillations resulting from the first three disturbances were of moderate amplitude. At a Mach number of approximately 0.9 after the elevator deflected to -4.2° , the model pitched up to the stall lift coefficient as indicated by increasing angle of attack with no corresponding increase in lift coefficient (at time = 6.35 seconds). When the elevator deflected back to -1.6° , the model recovered from the stall but, at a Mach number of approximately 0.7, when the elevator returned to -4.2° , the model pitched up through the stall to angles of attack considerably above the angle-of-attack-indicator range. During the portion of flight previous to 8.9 seconds the transverse accelerations were of small magnitude (maximum of $\frac{1}{2} g$) and the rates of roll and yaw were too small to be measured by the instrumentation used.

Subsequent to 8.9 seconds (at which time the 25° limit of the angle-of-attack indicator was exceeded) it was not possible to obtain accurate values of Mach number or dynamic pressure. For that reason the time history shown in figure 7 is not presented in coefficient form. However, the important basic quantities measured between 8.4 and approximately 12.0 seconds are presented in figure 7 to illustrate qualitatively the behavior of the model after the angle-of-attack-indicator range was exceeded.

Beginning at 8.9 seconds the angle of attack exceeded 25° , the sum of the roll velocity squared and yaw velocity squared, $(\dot{\phi})^2 + (\dot{\psi})^2$ oscillated between values of 0 and roughly 300 (rad/sec)^2 and the oscillation in the time history of this quantity was in phase with an oscillation in the normal acceleration time history (that is, when the yaw and roll velocities were maximum the normal acceleration was maximum). The time history obtained during this interval is what one might expect from a model in a Dutch-roll or falling-leaf type of maneuver while at a very high angle of attack.

The angle-of-attack indicator remained against the 25° stop until 9.75 seconds where the angle of attack dropped momentarily below 25° , apparently as a result of the tail deflecting to the -1.6° position. The model did not recover from the high-angle-of-attack maneuver at that time but seemingly continued the Dutch-roll type of maneuver at a lower level of normal acceleration until 10.4 seconds after firing.

When the tail deflected to -4.2° at approximately 10.4 seconds, the angle of attack began to oscillate from stop to stop in phase with a high-amplitude oscillation in normal acceleration and the quantity $(\dot{\phi})^2 + (\dot{\psi})^2$ became comparatively steady at an average level between 300 and 350 (rad/sec)^2 . At the same time the transverse acceleration time history began to oscillate over a much greater range. It is believed that the model started rolling at approximately 10.4 seconds, that its longitudinal axis remained at a high and comparatively constant angle in space and that the rate of roll was equal to the square root of the average value of $(\dot{\phi})^2 + (\dot{\psi})^2$ between 10.5 and 11.3 seconds. The maximum rate of roll attained as indicated by this method and as substantiated by the angle of attack indicator "oscillation" was approximately 18.5 radians per second. Apparently the rate of roll began to decrease at approximately 11.1 seconds and the model recovered from this maneuver near the time the tail deflected to the lower tail setting at 11.5 seconds.

Since the model and full-scale airplane are not dynamically similar, the model motions between 8.9 and 11.1 seconds may not be entirely indicative of the violence of motions that the airplane would experience. The model performance indicates, however, that the airplane configuration would be highly unsatisfactory and would probably perform comparable maneuvers under similar conditions of angle of attack and Mach number. The type of roll maneuver experienced by the model would result in very high yaw angles and vertical-tail side force coefficients.

As noted in a previous section, between 8.9 and 11.8 seconds the longitudinal and transverse acceleration readings were subject to possible position errors of from 1 to 2g. The Mach number at

11.4 seconds after firing was estimated to be approximately 0.25 which indicates a rapid decrease in speed during the entire sequence of maneuvers beginning at 8.9 seconds.

During the remainder of the flight (not shown) which was at low Mach numbers, the model pitched through a low range of normal acceleration with a period of oscillation approximately equal to the pulse rate of the horizontal tail. The rates of roll and yaw returned to values too small to be measured by the instrumentation used.

As indicated on figures 6 and 7 the model experienced buffeting at the higher lift coefficients. This was indicated by unusually shaky telemeter traces as shown in figure 8 which is a portion of telemeter record of α , δ , a_n/g , a_l/g and free-stream total pressure just previous to and during part of the flight where buffeting was encountered.

Lift

In figure 9 are presented variations of lift coefficient C_L with angle of attack α determined from the first one-half or first complete cycle of each of the oscillations illustrated in figure 6. The deviation in Mach number from the average Mach number of these data may be ascertained from figure 6 and, in the case of data taken near a Mach number of 0.7, the variation is indicated on figure 9. Except for data obtained from portions of flight where the model pitched through the stall condition the deviations of Mach number from the average indicated in the table of figure 9 were small (the order of ± 0.01).

As in the case of the model of reference 1, in general slightly different values of angle of attack, for a given value of lift coefficient, were obtained, depending on whether the angle of attack was increasing or decreasing with time. This hysteresis effect is evident in figure 9 (where data were obtained with angle of attack both increasing and decreasing) in the form of a loop. The loop indicated in the data obtained near 0.9 Mach number was due mainly to the usual separation effect occurring at the stall. Part of the loop in this and the other C_L against α plots can also be accounted for by other aerodynamic effects. For instance it is known that a lift arises from the rate of change of angle of attack with time. It is believed that this small amount of hysteresis (in the case of data taken from oscillations entirely below the stall) does not affect the slopes of the curves of C_L against α .

From figure 9 it can be seen that the variation of lift with angle of attack was somewhat nonlinear even at low angles of attack. This was also true of corresponding data from the model of reference 1.

The lift-curve slope values obtained from the plots of figure 9 for the model below the stalled condition are shown in figure 10 along with the variation with Mach number of the average lift curve obtained from these values and the average lift-curve slope shown in reference 1. In general the agreement between the lift-curve slope data from the present model and model of reference 1 is good.

Drag

A limited number of values of the minimum total drag coefficient C_{Dmin} were obtained from this model. These values are shown in figure 11 along with the variation of C_{Dmin} with Mach number from the model of reference 1. The agreement between models is good.

The drag polars C_D against C_L obtained from this model are presented in figure 12. The points shown on these plots correspond to the points in the C_L against α data in figure 9. The polars obtained for this model show that the minimum drag was experienced at lift coefficients between 0.05 and 0.12 throughout the Mach number and tail-deflection ranges covered. This is in disagreement with results obtained with the model of reference 1 as evidenced by the comparison of the polars obtained near a Mach number of 0.7 from each of the models (see fig. 12). The disagreement between the models has not been satisfactorily explained but may be at least partially due to an undetermined aerodynamic asymmetric effect on one or both of the angle-of-attack indicators used.

It should be noted that all values of C_D presented in figures 11 and 12 include C_D due to air flow through the ducts.

Longitudinal Stability

Static stability.- All pitch oscillations induced by the tail movement wherein the stall lift coefficient was not exceeded were analyzed by the methods of reference 2. The variation of the period of these oscillations with Mach number is shown in figure 13(a). Variation of the static stability parameter $C_{m\alpha}$ with Mach number as obtained from the faired curve of figure 13(a) is presented in figure 13(b). The aerodynamic-center location, throughout the Mach number range, as calculated by dividing $C_{m\alpha}$ by average Cl_{α} , is shown in figure 13(c) along with the corresponding average data of reference 1. The lift coefficients at which these data were obtained on the present model corresponded approximately to the average lift coefficient of the model of reference 1.

The variation of static pitching-moment coefficient with angle of attack near 0.7 Mach number, obtained by a method described briefly in the Test and Analysis section, is shown in figure 14. This curve shows that the model was stable up to an angle of attack of 9.4° . The model was apparently unstable between this angle of attack and an angle of attack of 25° where the indicator went against the stop; however, the degree of instability was considerably less beyond an angle of attack of 14° . Examination of the time-history plot in figure 7 indicates the model must have become stable at some angle in excess of 25° since it apparently reached a trim condition. The trim angle of attack has been estimated to be roughly 45° at a time of 9.25 seconds after firing. This was done by assuming a constant variation of a_n/g with angle of attack between 8.8 and 9.25 seconds.

Damping in pitch.- Rate of decay of the pitch oscillations of this model is shown in figure 15(a) in terms of time to damp to one-half amplitude, $T_{1/2}$. A faired line through these points was used to obtain the variation of the total damping term $K_2/T_{1/2}$ with Mach number (fig. 15(b)). This total damping term was subtracted from the lift term $K_1 C_{L_\alpha}$ to obtain the damping coefficient $C_{mq} + C_{m\dot{\alpha}}$ presented in figure 15(c). A plot of $C_{mq} + C_{m\dot{\alpha}}$ from the model of reference 1 is also shown. Comparison of $C_{mq} + C_{m\dot{\alpha}}$ from the two models shows serious disagreement only at the higher Mach numbers. This disagreement stems primarily from the disagreement between the total damping terms $K_2/T_{1/2}$, which in turn was a result of the difference in $T_{1/2}$ measured at one point ($M = 1.15$). Part of this difference is due to the difference in center-of-gravity location (difference = 15.4 percent \bar{c}), as illustrated by the difference in the values of damping coefficient calculated by the method of reference 4 and shown in figure 15(c). In light of the curves obtained from reference 4 it seems that the damping-coefficient data obtained from the model of reference 1 are more indicative (at least above $M = 1.1$) of the damping characteristics of the configuration, although data from the present model were of comparable quality and were obtained at approximately the same lift coefficients.

Trim

The variation with Mach number of trim angle of attack and lift coefficient for this configuration (tail of aspect ratio = 3.0) as obtained from the present model at two horizontal tail deflections is shown in figure 16. The solid lines indicate where data were obtained alternately at the two tail settings. The cross-hatched bands indicate that the trim could only be determined approximately because the model was near the stall and trim was indefinite. The trim point at $M \approx 0.7$ was obtained from the curve of figure 14.

The trim change indicated for the configuration with $\delta = -4.2^\circ$ is not serious when viewed along with the curve of airplane C_L for level flight at 40,000 feet altitude and $\frac{W}{S} = 120$ shown on the figure.

Directional Stability

Lateral accelerations of this model were very low previous to the time the model became unstable. There were, however, small amplitude lateral oscillations and the periods of these oscillations were as shown in figure 17(a). The method of reference 5 was used to determine $C_{n\beta}$ values which are shown in figure 17(b) along with corresponding data from the model of reference 1. As may be seen from this figure, the $C_{n\beta}$ values from this model were considerably lower than those from the model of reference 1. Approximately one-third of the difference in these data from the two models may be attributed to the difference in center-of-gravity position. It should be noted that on the present model lateral accelerations were obtained by the use of continuous telemetering channels, whereas a switched channel system was used to obtain lateral acceleration data on the model of reference 1. Because of the low switching rate, the data from model of reference 1 show considerably more scatter than that from the present test.

Also shown in figure 17(b) are values of $C_{n\beta}$ as obtained from data on this configuration tested in the Ames 6- by 6-foot supersonic tunnel at a Mach number of 0.9 and Reynolds number of 2.29×10^6 (unpublished data). One of these values was obtained over angle-of-yaw range of $\pm 0.5^\circ$ and the other which agrees well with data from the present tests was obtained at an angle of yaw of about 4° . The lower value of $C_{n\beta}$ obtained from the tunnel tests over angle-of-yaw range of $\pm 0.5^\circ$ is possibly due to an effect of low Reynolds number on the transition point of the flow over the vertical tail. The Reynolds numbers of the rocket-model tests at this Mach number were between 6.5×10^6 and 7.1×10^6 .

Comparison with Wind-Tunnel Tests

Shown in figure 18 are comparisons in lift, drag, and pitching-moment data from the present model test and from tests on a similar model in the Ames 12-foot pressure wind tunnel (unpublished data).

Reynolds number of the tunnel test data was 1.1×10^6 , whereas rocket test Reynolds number in this Mach number range was approximately 3.7×10^6 . Drag data from both rocket and tunnel models include

~~CONFIDENTIAL~~

internal duct drag. Tunnel model base pressure was corrected to atmospheric pressure. No base pressure measurements were made on the rocket model.

In general, agreement between the rocket-model and wind-tunnel tests is very good.

CONCLUDING REMARKS

A rocket-propelled model of the X-3 equipped with an all-movable tail of aspect ratio 3.0 and with open ducts has been flown primarily to obtain the longitudinal characteristics at high lift coefficients and at high subsonic Mach numbers.

The most significant result obtained was that the model became unstable at lift coefficients above the stall at a Mach number of approximately 0.7 and that, at lift coefficients considerably higher than the stall, the model went into an erratic yaw-roll maneuver from which the model recovered only after the Mach number had decreased to approximately 0.25. During part of this maneuver, while the longitudinal axis of the model was at a high and comparatively constant angle in space, the model rolled rapidly so that the wing, horizontal tail, and vertical tail surfaces were subjected to very high amplitude variations in angle of attack and sideslip. The data obtained at lower lift coefficients throughout a Mach number range from 0.7 to 1.2 in general agreed reasonably well with corresponding data from the model of reference 1.

Langley Aeronautical Laboratory
National Advisory Committee for Aeronautics
Langley Field, Va.

REFERENCES

1. Mitchell, Jesse L., and Peck, Robert F.: An Investigation of the Longitudinal Characteristics of the X-3 Configuration Using Rocket-Propelled Models. Preliminary Results at Mach Numbers from 0.65 to 1.25. NACA RM L50J03, 1950.
2. Gillis, Clarence L., Peck, Robert F., and Vitale, A. James.: Preliminary Results from a Free-Flight Investigation at Transonic and Supersonic Speeds of the Longitudinal Stability and Control Characteristics of an Airplane Configuration with a Thin Straight Wing of Aspect Ratio 3. NACA RM L9K25a, 1950.
3. Mitchell, Jesse L., and Peck, Robert F.: An NACA Vane-Type Angle-of-Attack Indicator for Use at Subsonic and Supersonic Speeds. NACA RM L9F28a, 1949.
4. Harmon, Sidney M.: Stability Derivatives at Supersonic Speeds of Thin Rectangular Wings with Diagonals ahead of Tip Mach Lines. NACA Rep. 925, 1949. (Formerly NACA TN 1706.)
5. Bishop, Robert C., and Lomax, Harvard: A Simplified Method for Determining from Flight Data the Rate of Change of Yawing-Moment Coefficient with Sideslip. NACA TN 1076, 1946.

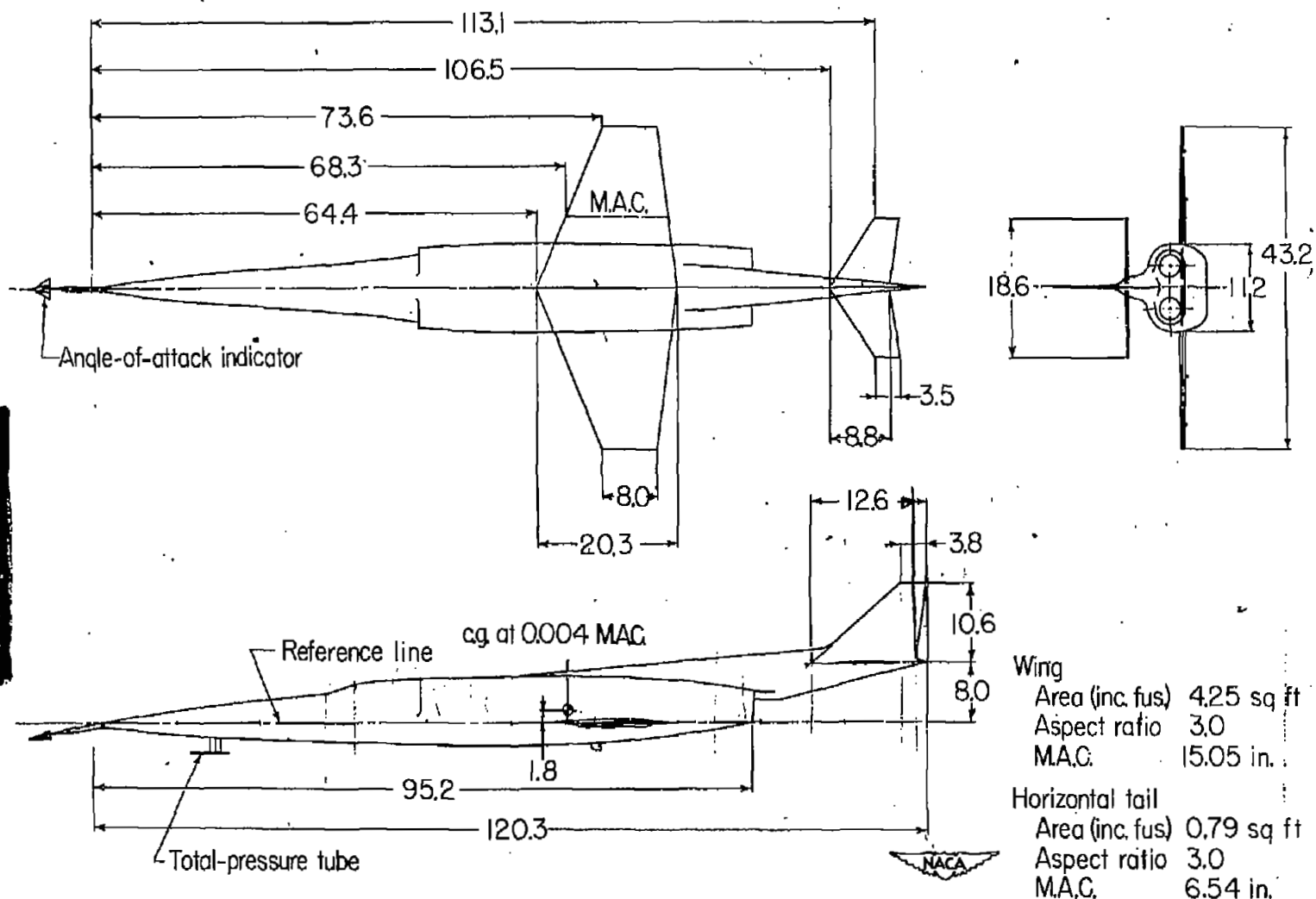
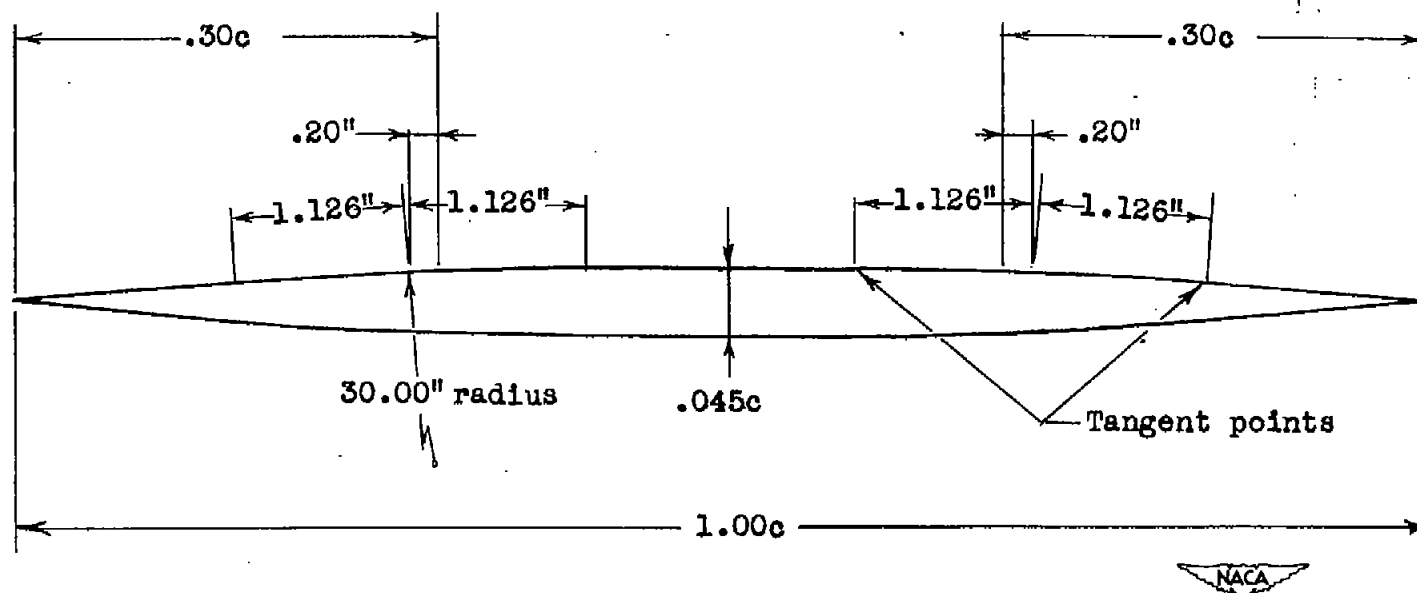


Figure 1.- General arrangement of X-3 model. All dimensions are in inches.



Note: Leading and trailing edge radii $\approx 0.015''$

Figure 2.- Typical airfoil section of all surfaces on rocket-propelled X-3 model.

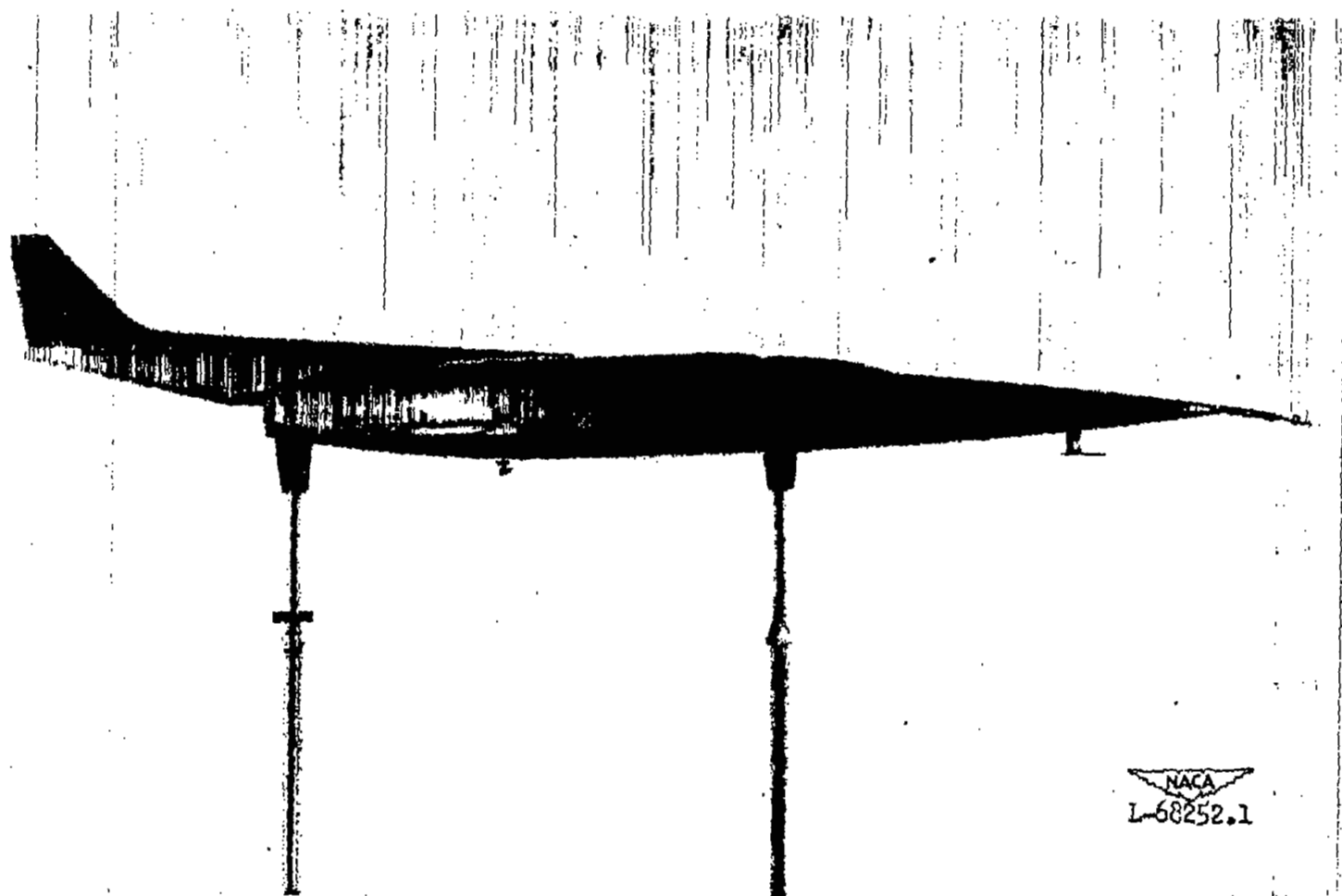


Figure 3.- Photographs of X-3 model.

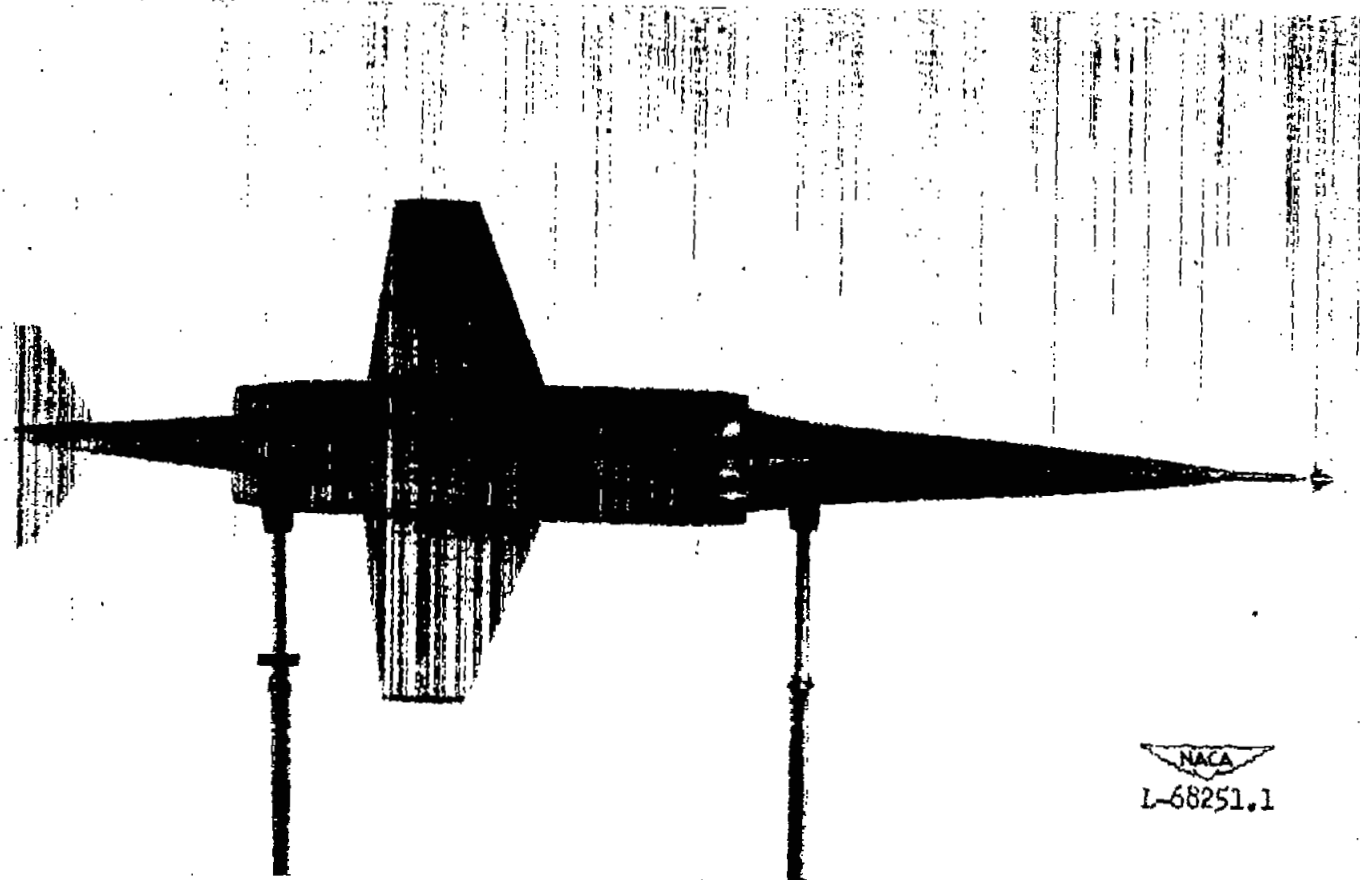


Figure 3.- Concluded.

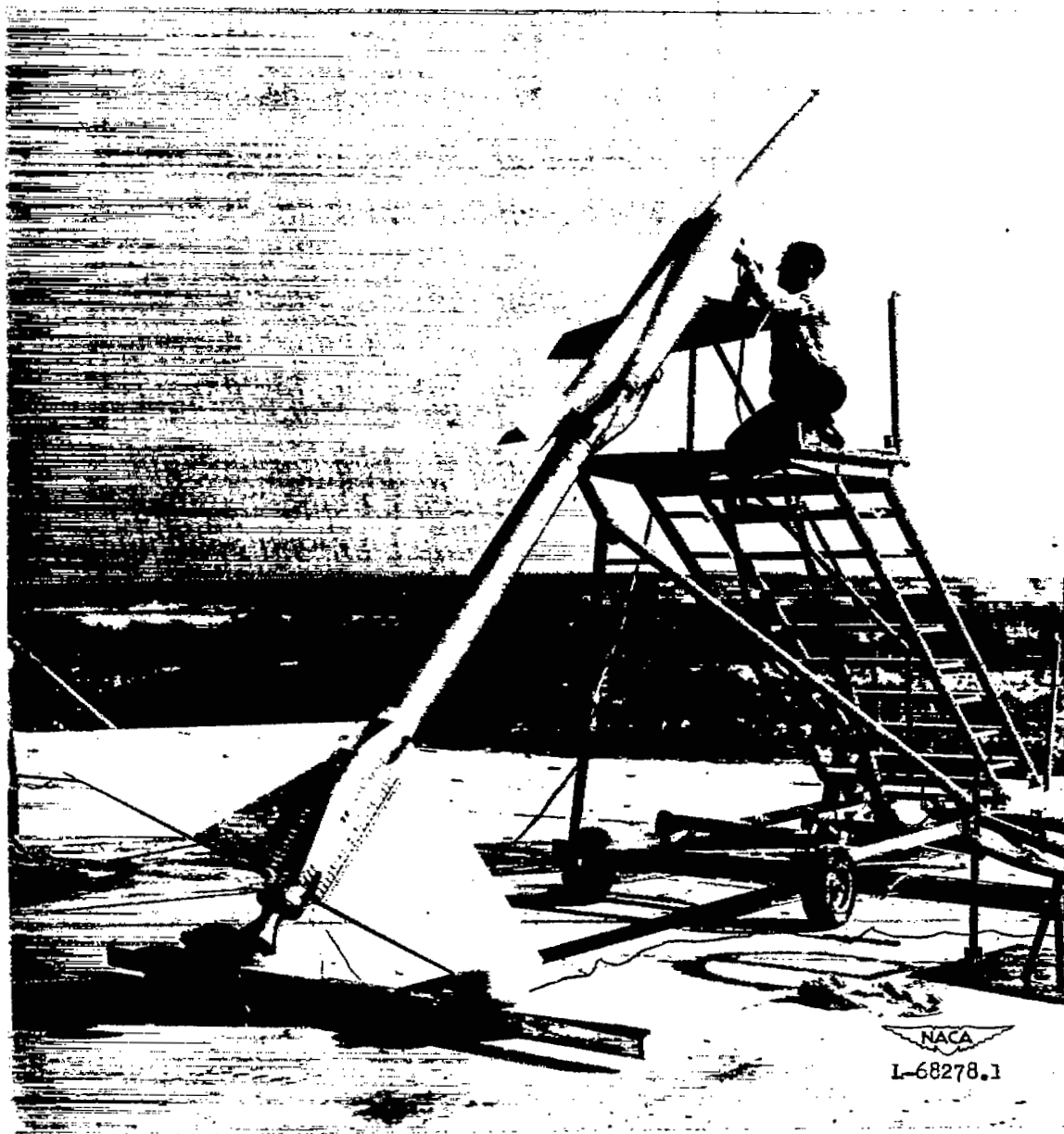


Figure 4.- Photograph of X-3 model and booster.

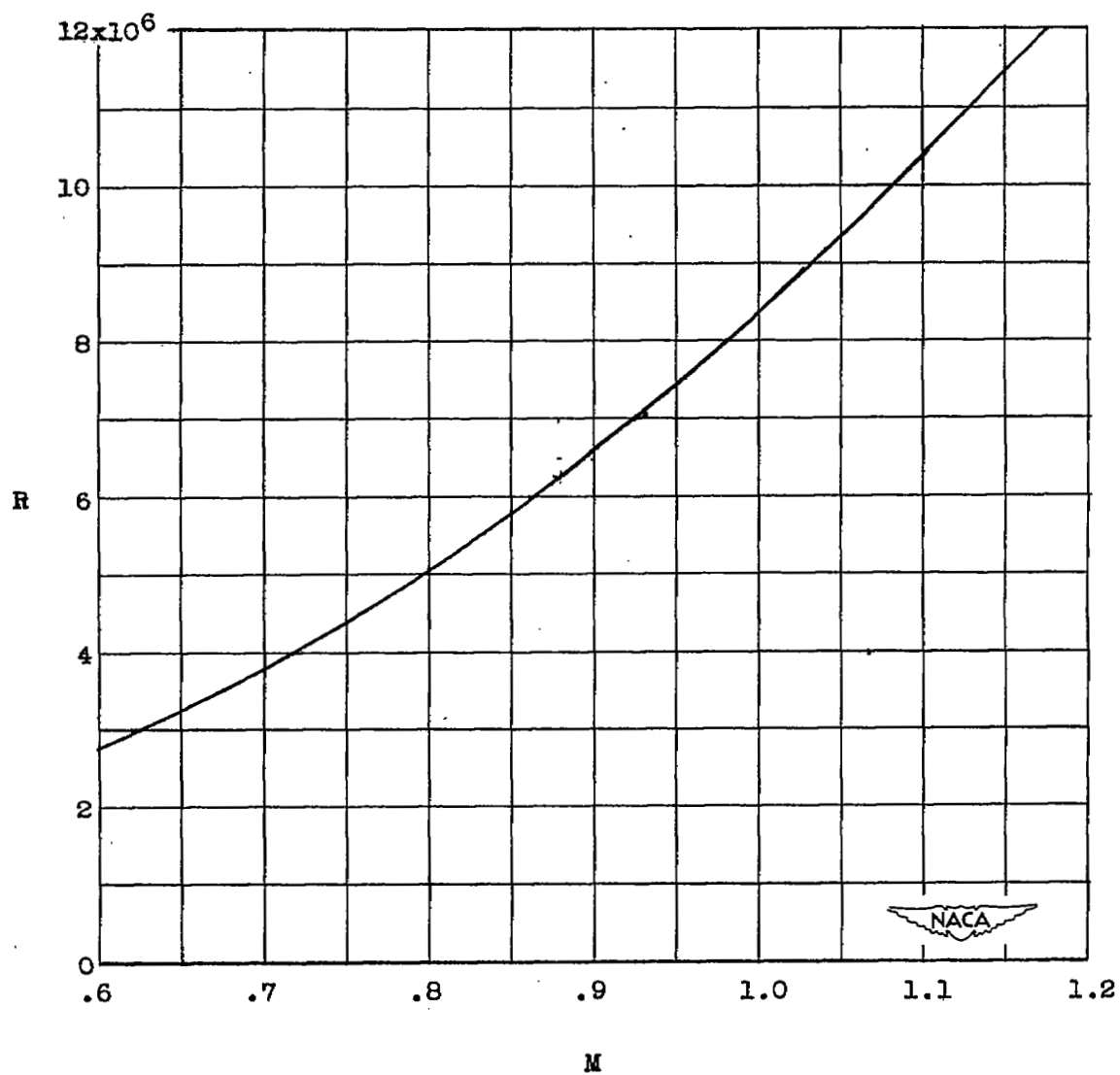


Figure 5.- Test Reynolds number based on mean aerodynamic chord.

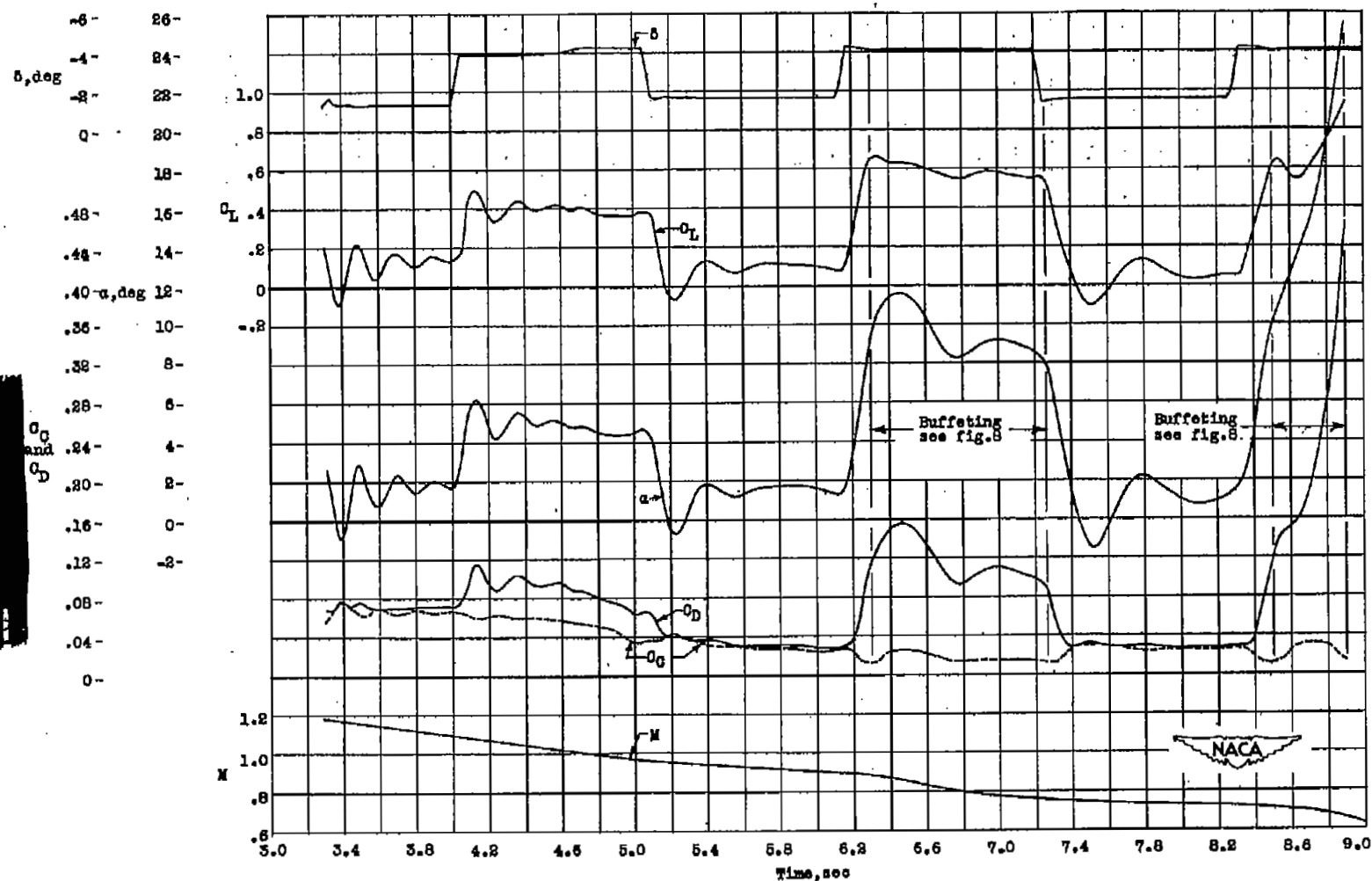


Figure 6.- Time history before angle-of-attack-indicator range was exceeded.

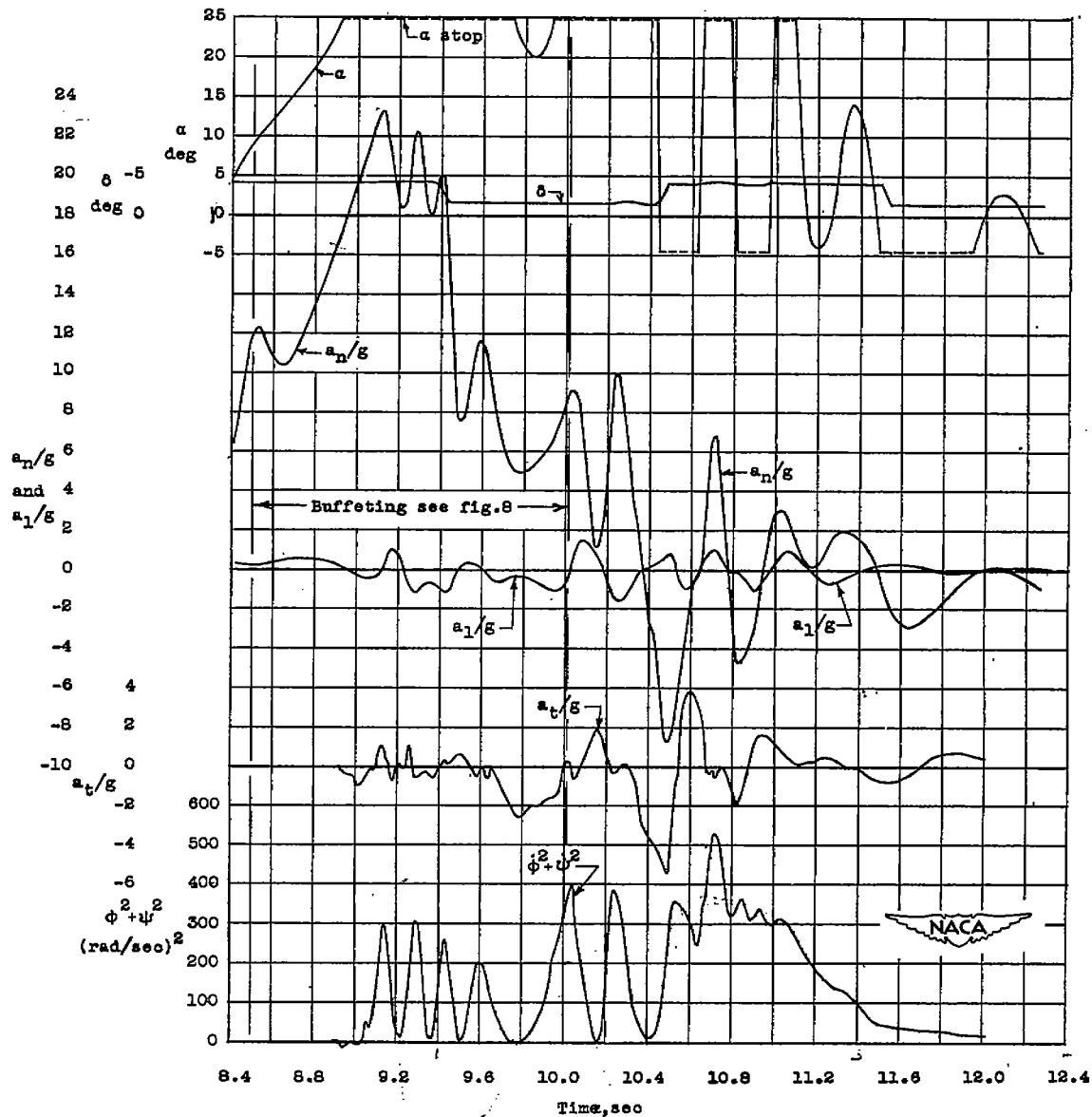


Figure 7.- Time history after angle-of-attack-indicator range was exceeded.

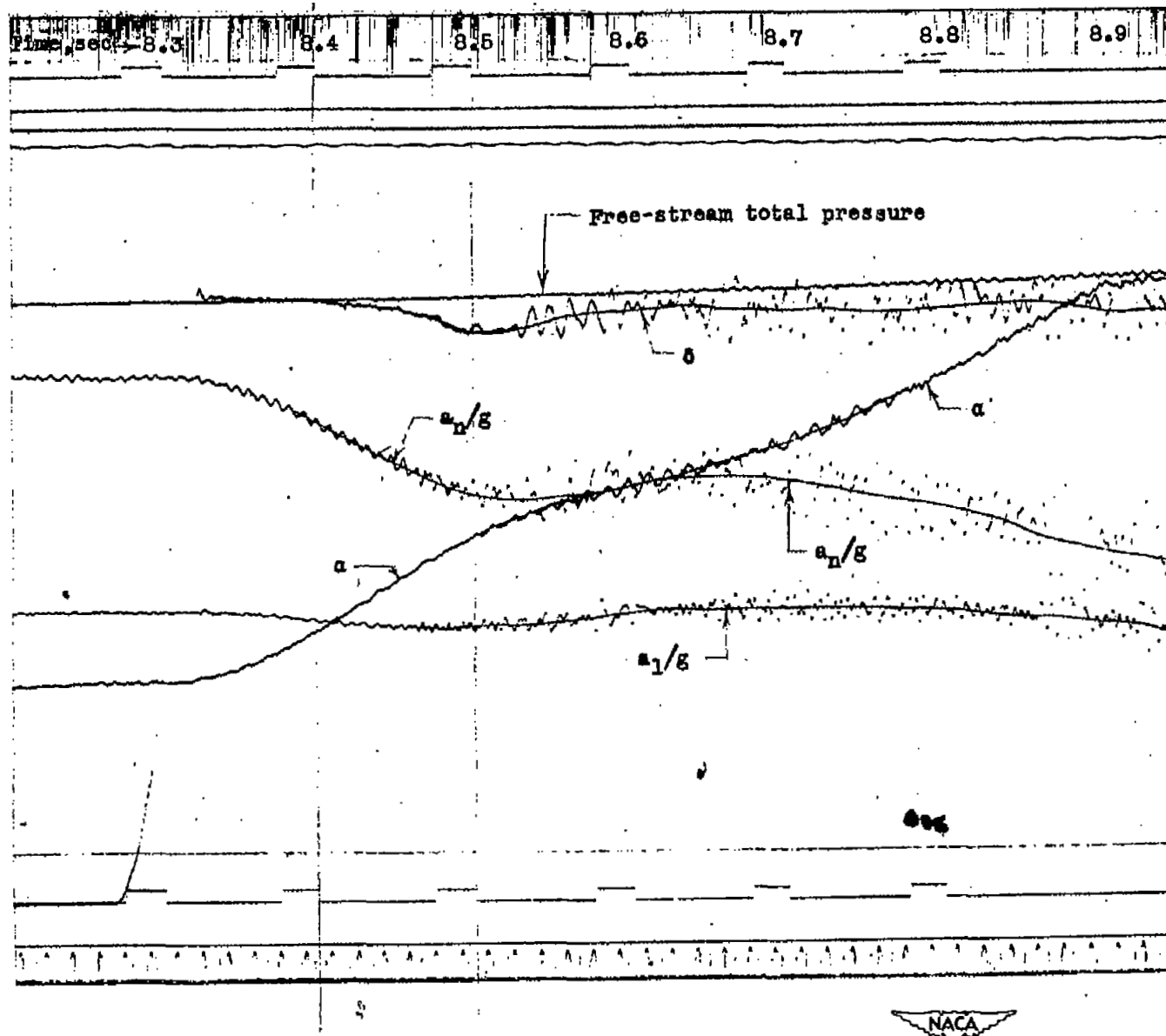


Figure 8.- Portion of telemetered record during buffeting.

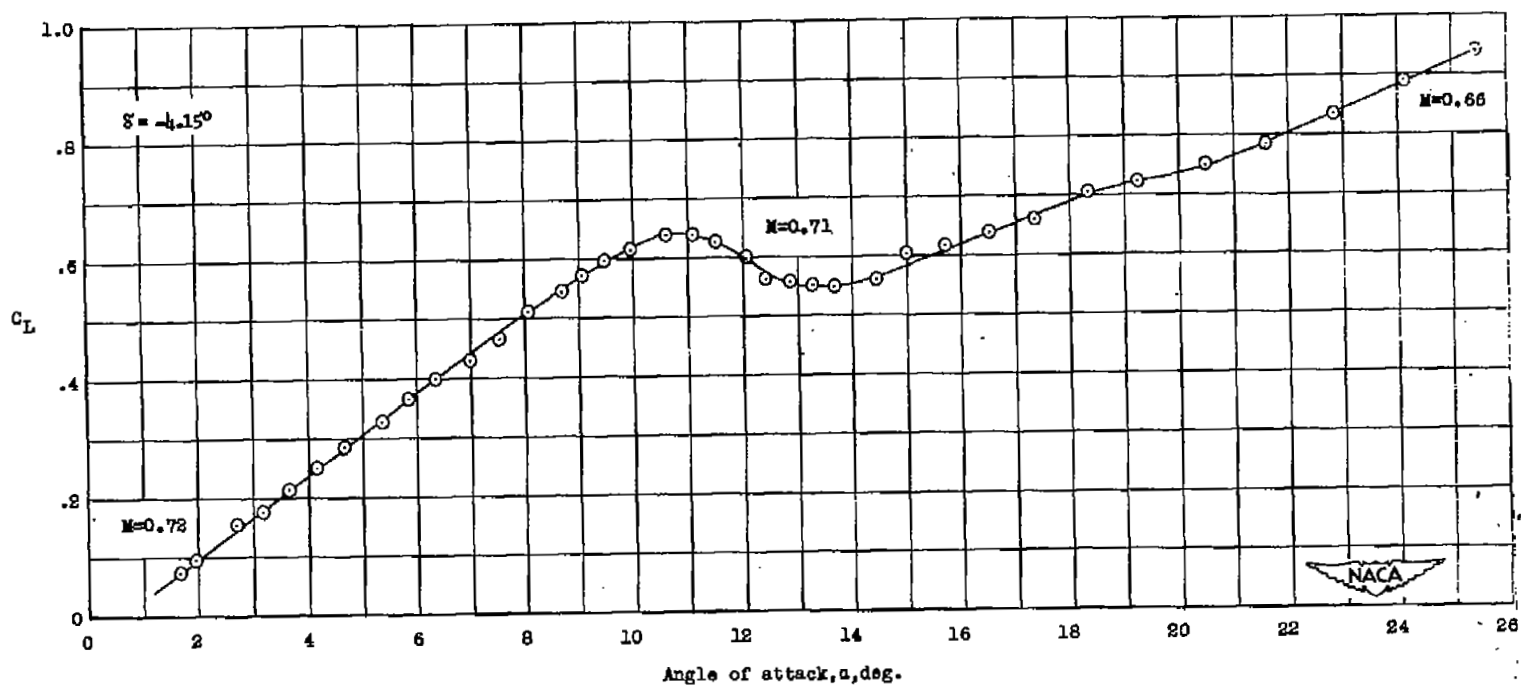


Figure 9.- Variation of lift coefficient with angle of attack.

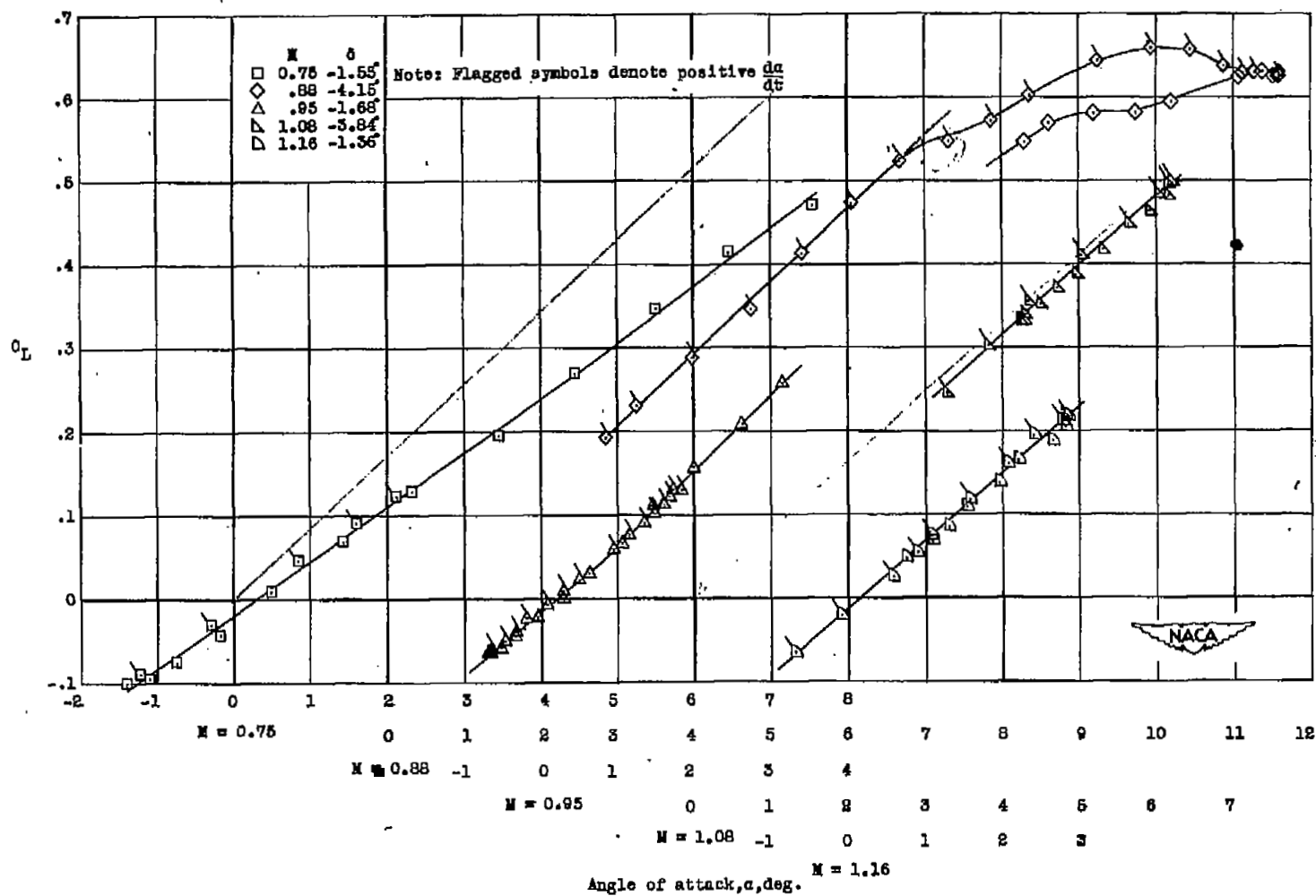


Figure 9.- Concluded.

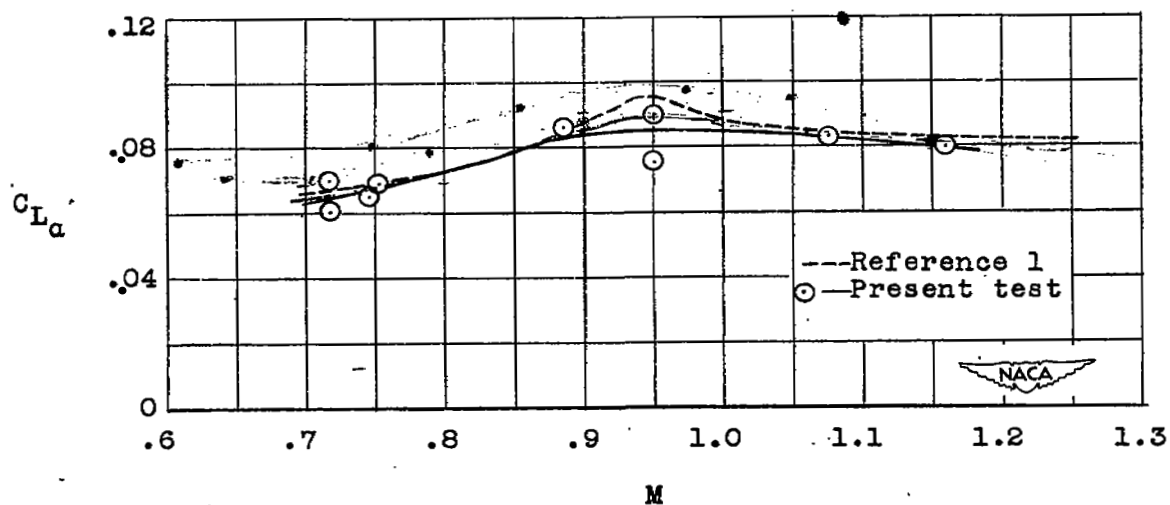


Figure 10.- Lift-curve slope.

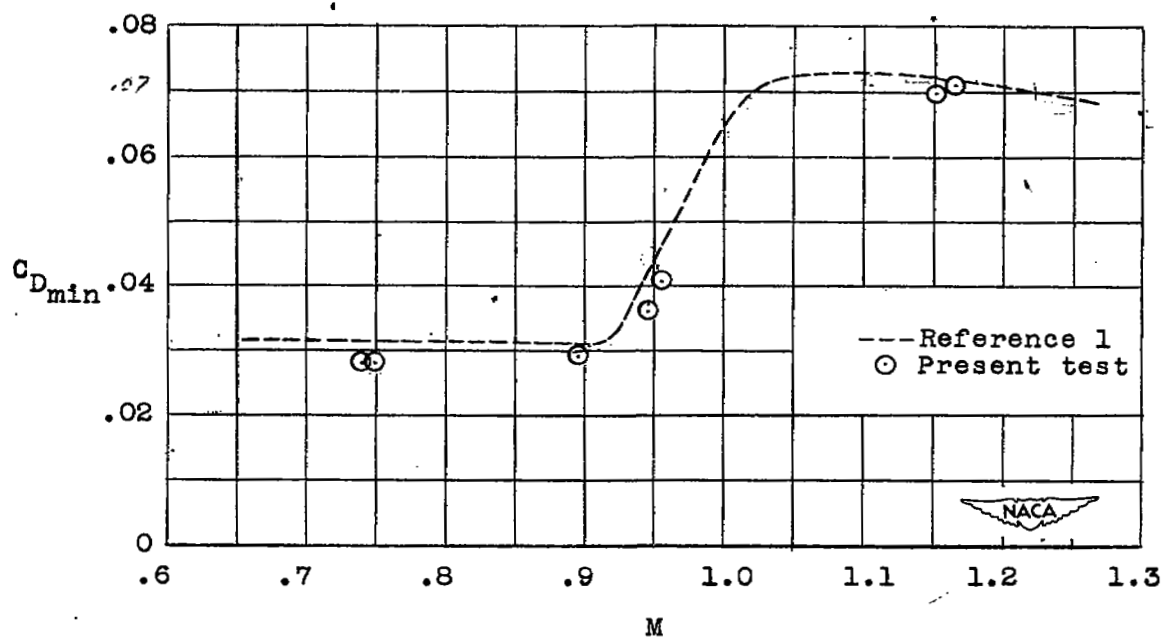


Figure 11.- Minimum drag coefficient.

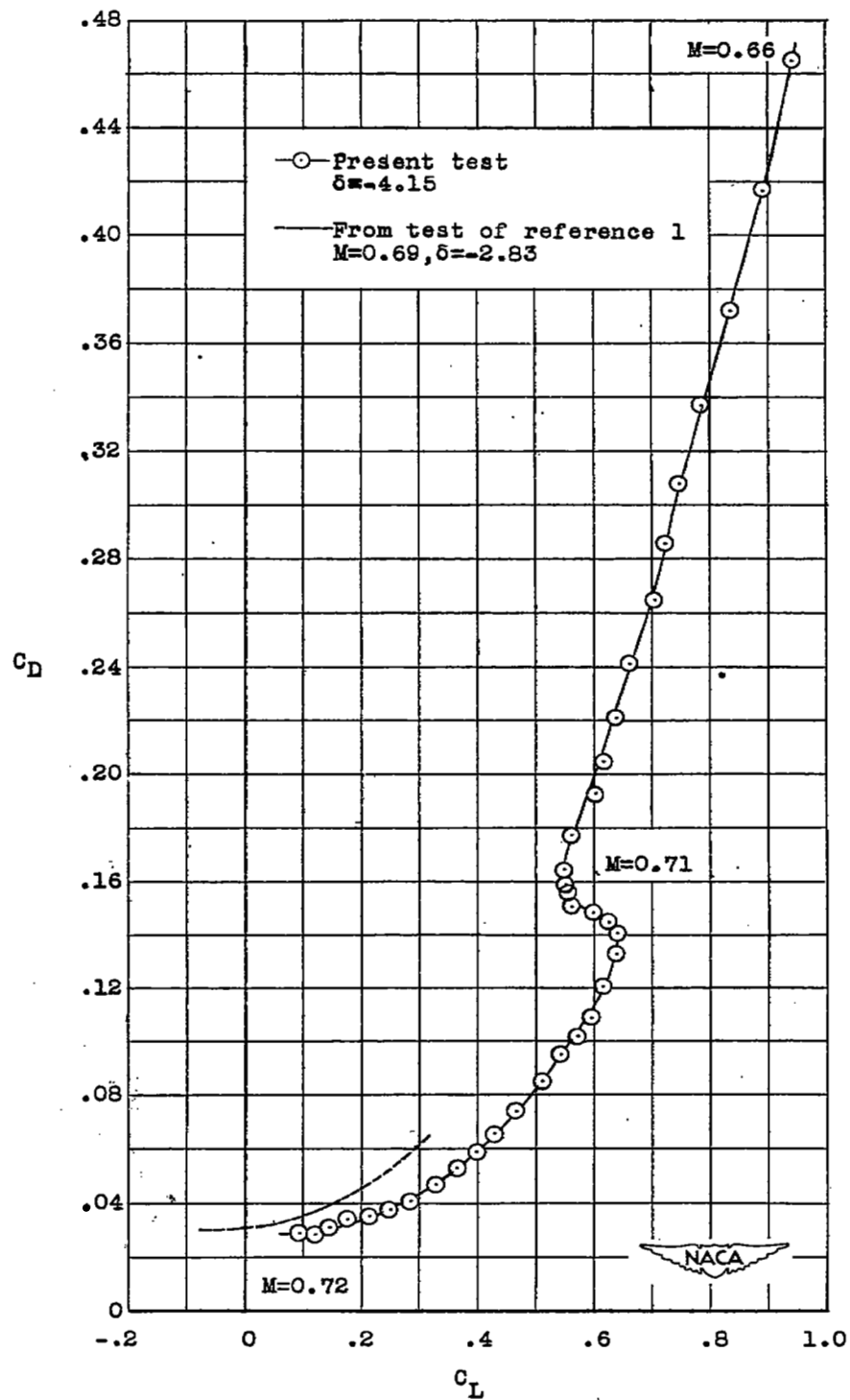


Figure 12.- Variation of drag coefficient with lift coefficient.

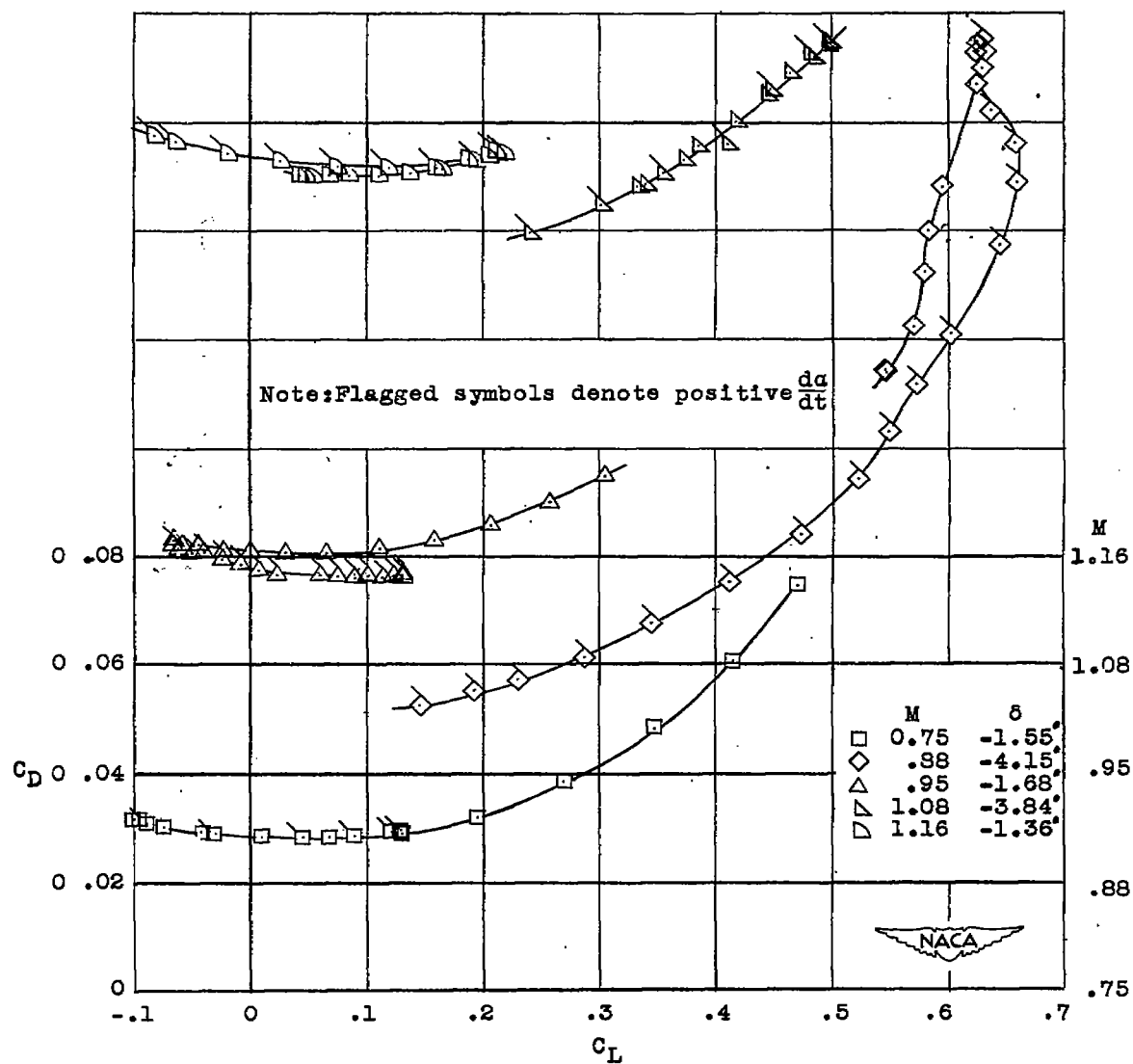
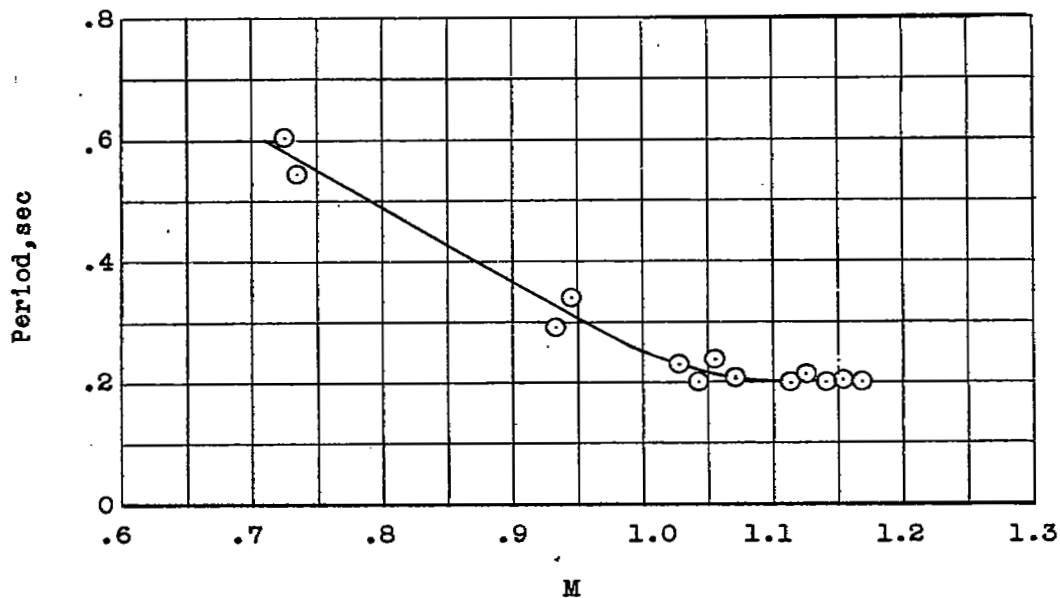
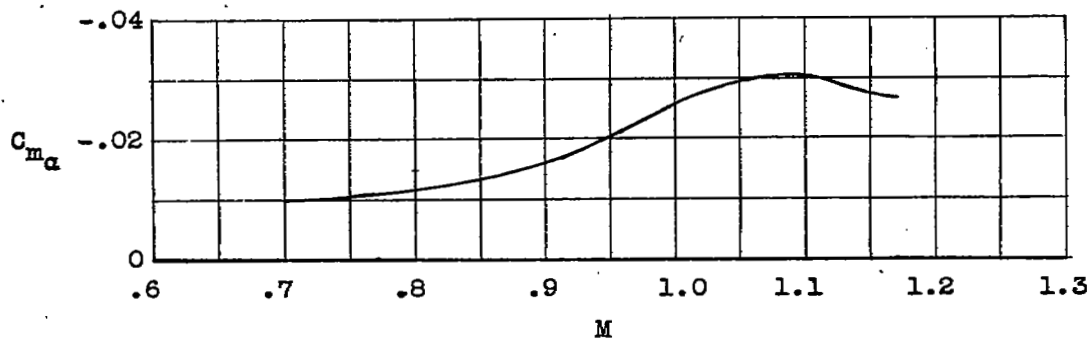
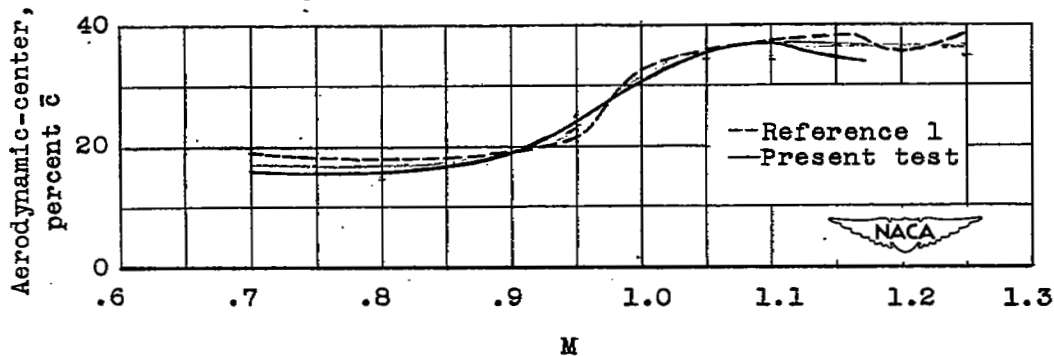


Figure 12.- Concluded.



(a) Period of longitudinal oscillation.

(b) Longitudinal stability parameter C_{m_α} with center of gravity at 0.4 percent M.A.C.

(c) Average aerodynamic-center location.

Figure 13.- Static longitudinal-stability characteristics.

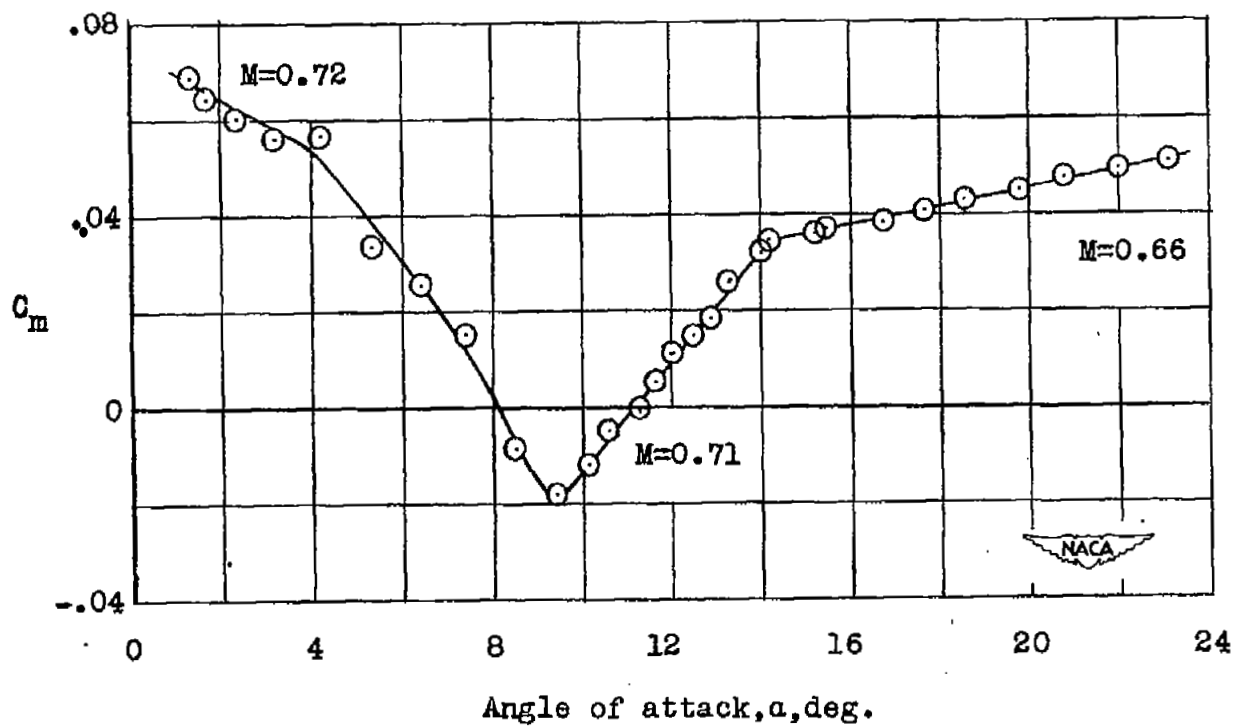
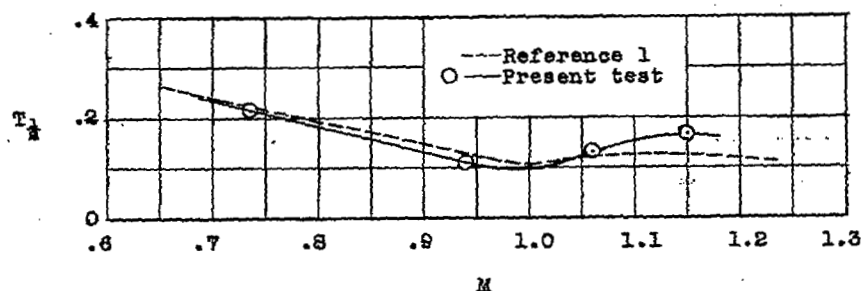
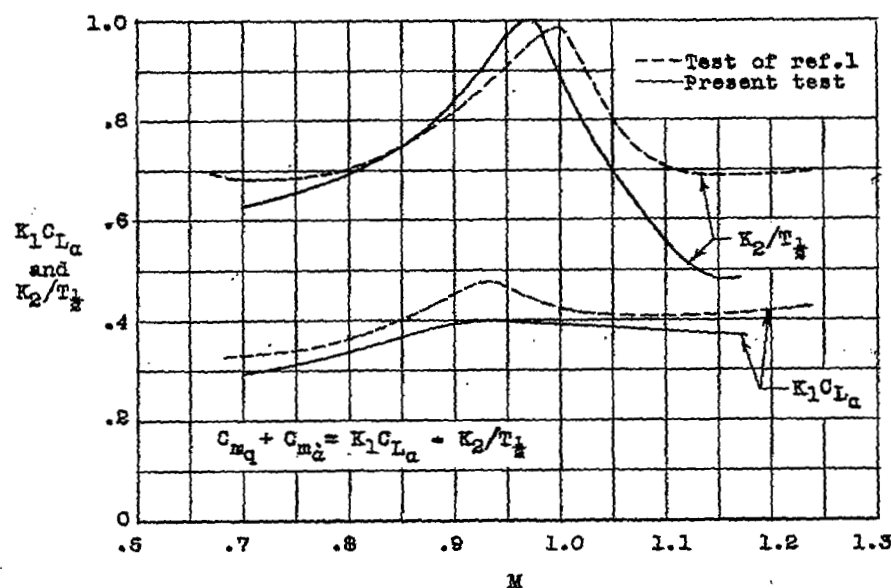


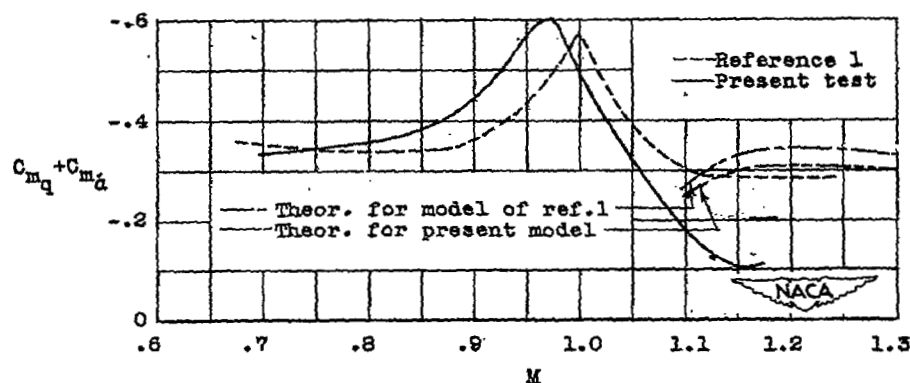
Figure 14.- Variation of static pitching-moment coefficient with angle of attack. Tail deflection = -4.15° .



(a) Time to damp to one-half amplitude.



(b) Total damping and lift damping factors.



(c) Pitching-moment damping factor.

Figure 15.- Damping characteristics of longitudinal short-period oscillation.

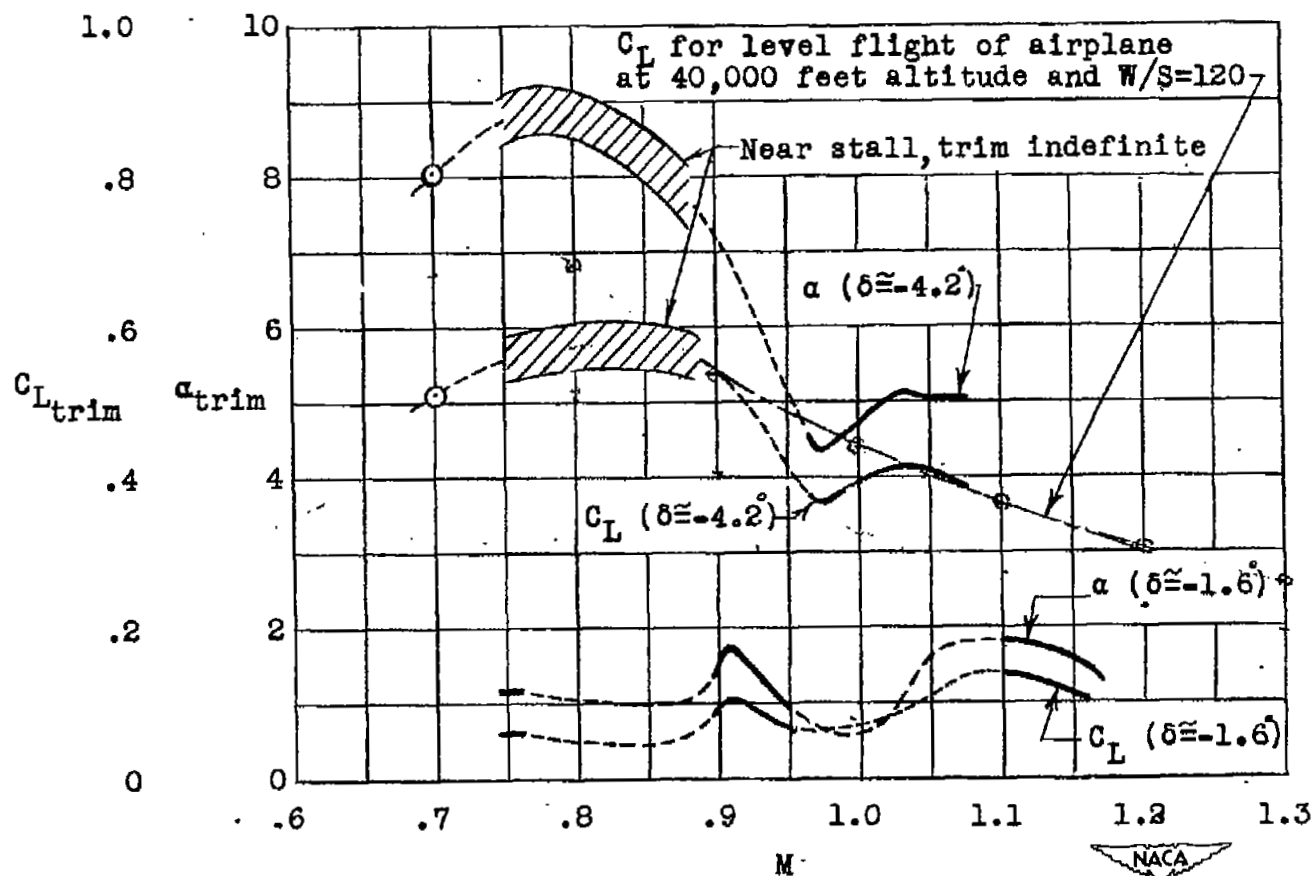
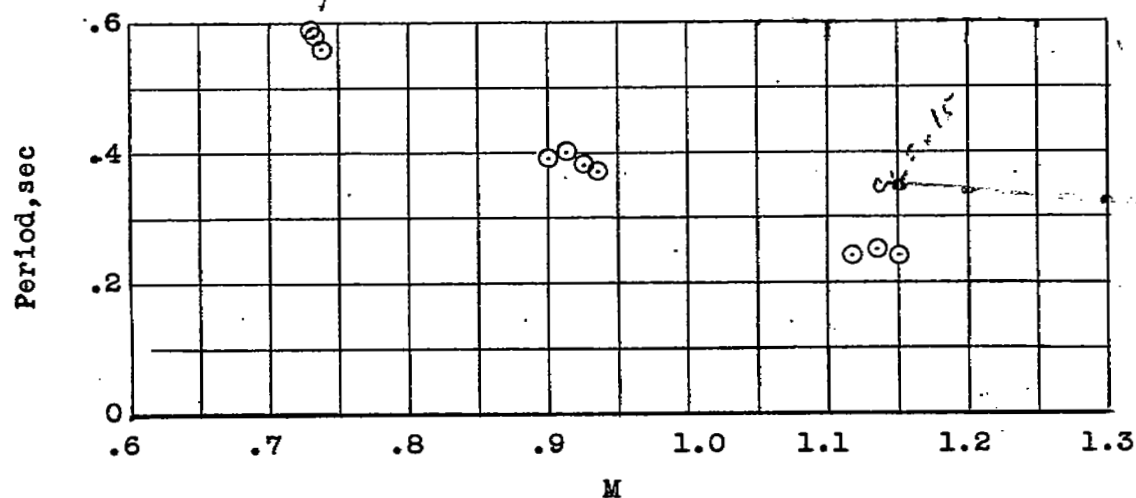


Figure 16.- Trim lift coefficient and angle of attack.



(a) Period of lateral oscillation.

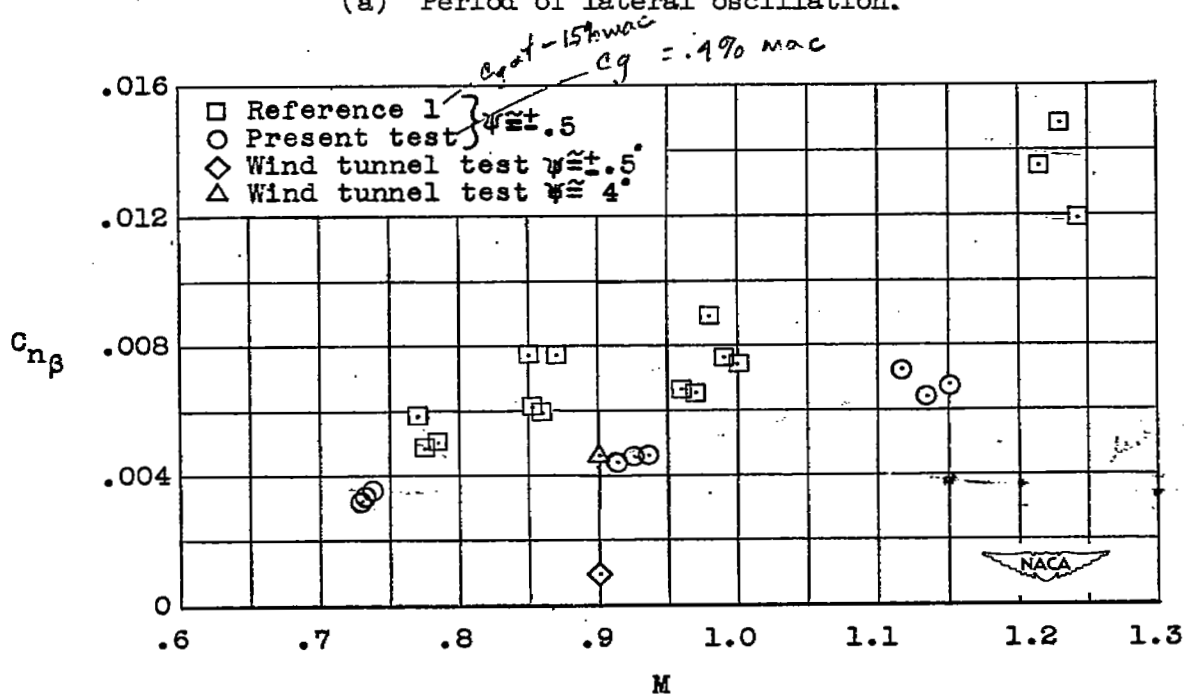
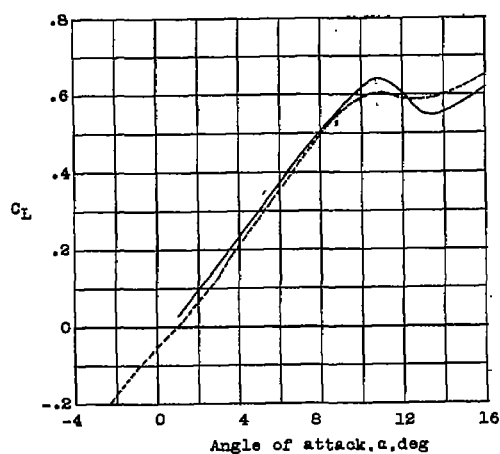
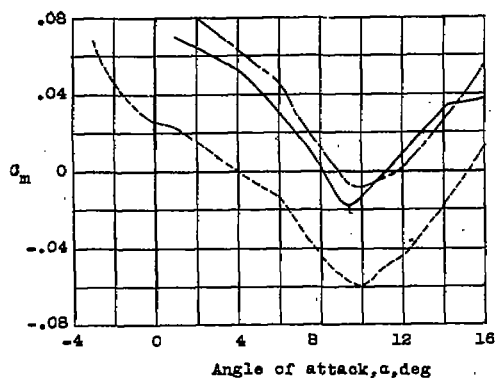
(b) Directional-stability parameter. $C_L \approx 1.5$

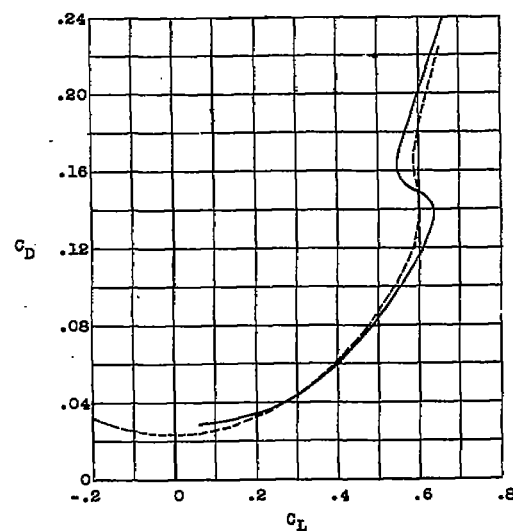
Figure 17.- Directional stability.



(a) Variation of lift coefficient with angle of attack.



(c) Variation of static pitching-moment coefficient with angle of attack.



(b) Variation of drag coefficient with lift coefficient.

— Present rocket model test
 $M=0.71, \delta=4.15$
 --- Wind tunnel test
 $M=0.70, \delta=2.2$
 - - - Estimated from wind tunnel test
 $M=0.70, \delta=4.15$



Figure 18.- Comparisons with wind-tunnel data.



3 1176 01436 4393

~~CONFIDENTIAL~~

SECURITY INFORMATION

~~CONFIDENTIAL~~

SECURITY INFORMATION

~~CONFIDENTIAL~~